Wilfried Elmenreich, J. Tenreiro Machado and Imre J. Rudas (Eds)

Intelligent Systems

at the Service of Mankind

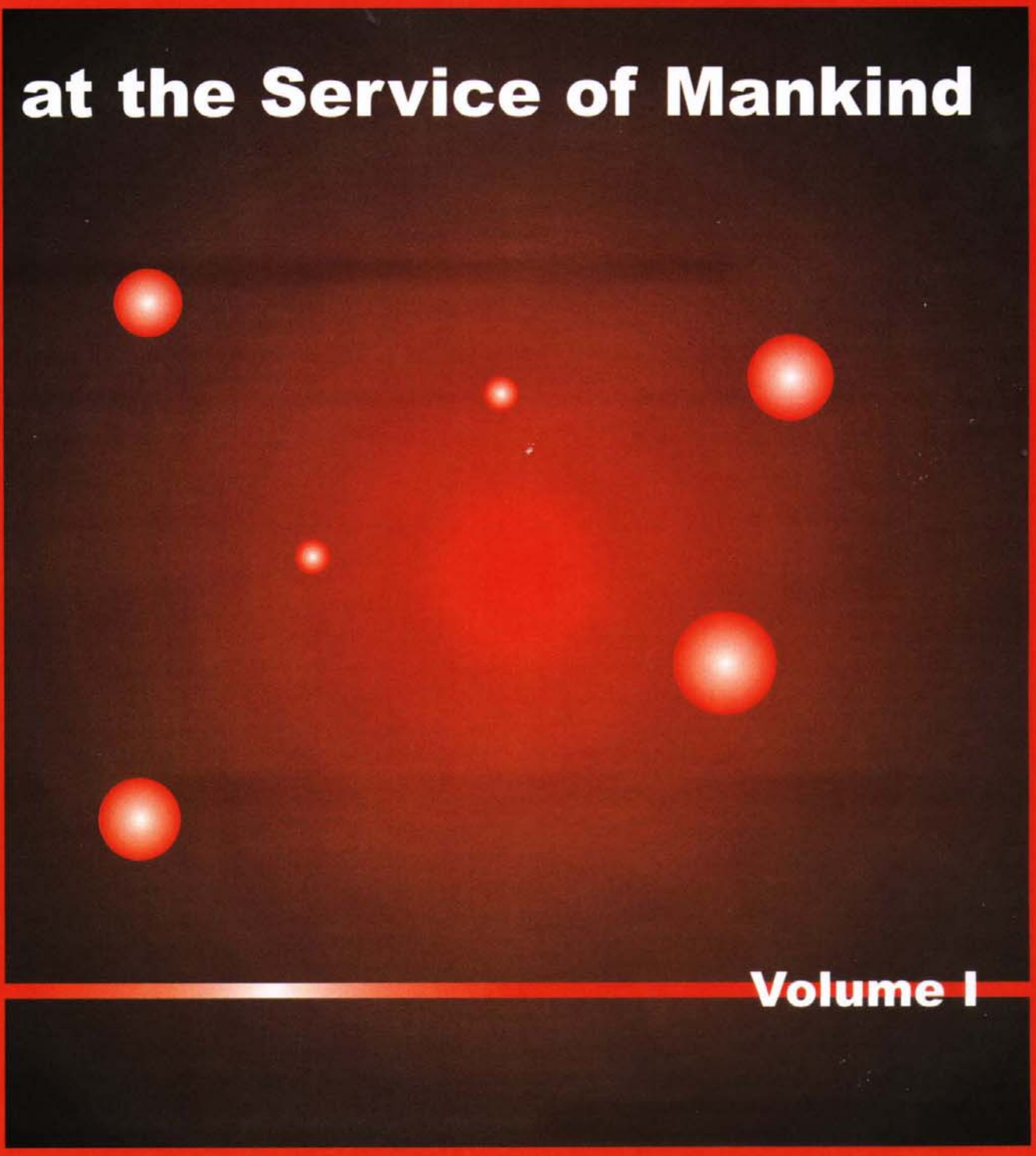

Volume I

Application of Fractional Calculus in Mechatronics

J. A. T. Machado[1], Ramiro Barbosa[1], Fernando Duarte[2], and Nuno Ferreira[3]

[1]Institute of Engineering,
Polytechnic Institute of Porto, Porto, Portugal
{jtm,rbarbosa}@dee.isep.ipp.pt

[2]School of Technology,
Polytechnic Institute of Viseu, Viseu, Portugal
{fduarte}@mat.estv.ipv.pt

[3]Institute of Engineering,
Polytechnic Institute of Coimbra, Coimbra, Portugal
{nunomig}@isec.pt

Abstract — *Fractional Calculus (FC) goes back to the beginning of the theory of differential calculus. Nevertheless, the application of FC just emerged in the last two decades. In the field of dynamical systems theory some work has been carried out but the proposed models and algorithms are still in a preliminary stage of establishment. Having these ideas in mind, the paper discusses a FC perspective in the study of the dynamics and control of mechanical systems.*

1 Introduction

The generalization of the concept of derivative $D^{\alpha}f(x)$ to non-integer values of α goes back to the beginning of the theory of differential calculus. In fact, Leibniz, in his correspondence with Bernoulli, L'Hôpital and Wallis (1695), had several notes about the calculation of $D^{1/2}f(x)$. Nevertheless, the development of the theory of Fractional Calculus (FC) is due to the contributions of many other mathematicians such as Euler, Liouville, Riemann and Letnikov [1–3]. In the fields of physics and chemistry [1], FC is presently associated with the modeling of electro-chemical reactions, irreversibility and electromagnetism. The adoption of the FC in control algorithms has been recently studied using the frequency and discrete-time domains [4–5]. Nevertheless, this research is still giving its first steps and further investigation is required.

Bearing these ideas in mind, this paper is organized as follows. Section 2 outlines the fundamental aspects of the theory of FC. Section 3 introduces the main algorithms to approximate fractional-order derivatives. Section 4 presents several case studies on the implementation of FC based models in the analysis and control of mechanical systems. Finally, section 5 draws the main conclusions.

2 Main Mathematical Aspects of the Theory of Fractional Calculus

Since the foundation of the differential calculus the generalization of the concept of derivative and integral to a non-integer order α has been the subject of several approaches. Due to this reason there are various definitions of fractional-order integrals (Table 1) which are proved to be equivalent [1–3].

Based on the proposed definitions it is possible to calculate the fractional-order integrals/derivatives of several functions. For example, according with [3] we have the formulae of Table 2. Nevertheless, the problem of devising and implementing fractional-order algorithms is not trivial and will be the matter of the next sections.

Riemann-Liouville	$\left(I_{a+}^{\alpha}\varphi\right)(x)=\frac{1}{\Gamma(\alpha)}\int_{a}^{x}\frac{\varphi(t)}{(x-t)^{1-\alpha}}dt,\ a<x,\ \alpha\in C$
Grünwald-Letnikov	$\left(I_{a+}^{\alpha}\varphi\right)(x)=\frac{1}{\Gamma(\alpha)}\lim_{h\to+0}\left[h^{\alpha}\sum_{j=0}^{[(x-a)/h]}\frac{\Gamma(\alpha+j)}{\Gamma(j+1)}\varphi(x-jh)\right]$
Laplace	$L\left\{I_{0+}^{\alpha}\varphi\right\}=L\{\varphi\}/s^{\alpha},\ \mathrm{Re}(\alpha)>0$

Table 1: Some definitions of fractional-order integrals

$\varphi(x),\ x\in R$	$\left(I_{+}^{\alpha}\varphi\right)(x),\ x\in R,\ \alpha\in C$
$(x-a)^{\beta-1}$	$\frac{\Gamma(\beta)}{\Gamma(\alpha+\beta)}(x-a)^{\alpha+\beta-1},\ \mathrm{Re}(\beta)>0$
$e^{\lambda x}$	$\lambda^{-\alpha}e^{\lambda x},\ \mathrm{Re}(\lambda)>0$
$\begin{cases}\sin(\lambda x)\\ \cos(\lambda x)\end{cases}$	$\lambda^{-\alpha}\begin{cases}\sin(\lambda x-\alpha\pi/2)\\ \cos(\lambda x-\alpha\pi/2)\end{cases},\ \lambda>0,\mathrm{Re}(\alpha)>1$
$e^{\lambda x}\begin{cases}\sin(\gamma x)\\ \cos(\gamma x)\end{cases}$	$\frac{e^{\lambda x}}{(\lambda^2+\gamma^2)^{\alpha/2}}\begin{cases}\sin(\gamma x-\alpha\phi)\ \ \phi=\arctan(\gamma/\lambda)\\ \cos(\gamma x-\alpha\phi)\end{cases},\ \gamma>0,\mathrm{Re}(\lambda)>1$

Table 2: Fractional-order integrals of several functions

3 Approximations to Fractional-Order Derivatives

In this section we analyze two methods for implementing fractional-order derivatives, namely the frequency-based and the discrete-time approaches, and its implication in control algorithms.

In order to analyze a frequency-based approach to D^{α}, with $\alpha\in R$ such that $0<\alpha<1$, let us consider the recursive circuit represented on Figure 1a:

$$I=\sum_{i=0}^{n}I_i,\ R_{i+1}=\frac{R_i}{\varepsilon},\ C_{i+1}=\frac{C_i}{\eta},\ \varepsilon,\eta>1 \tag{1}$$

where η and ε are scale factors, I is the current due to an applied voltage V and R_i and C_i are the resistance and capacitance elements of the i^{th} branch of the circuit.

The admittance $Y(j\omega)$ is given by:

$$Y(j\omega)=\frac{I(j\omega)}{V(j\omega)}=\sum_{i=0}^{n}\frac{j\omega C\varepsilon^{i}}{j\omega CR+(\eta\varepsilon)^{i}} \tag{2}$$

Figure 1b shows the asymptotic Bode diagrams of amplitude and phase of $Y(j\omega)$. The pole and zero frequencies (ω_i and ω'_i) obey the recursive relationships:

$$\frac{\omega'_{i+1}}{\omega'_i}=\frac{\omega_{i+1}}{\omega_i}=\varepsilon\eta,\ \frac{\omega_i}{\omega'_i}=\varepsilon,\ \frac{\omega'_{i+1}}{\omega_i}=\eta \tag{3}$$

From the Bode diagram of amplitude or of phase, the average slope m' can be calculated as:

$$m'=\frac{\log\varepsilon}{\log\varepsilon+\log\eta} \tag{4}$$

Consequently, the circuit of Figure 1a represents an approach to D^{α}, $0<\alpha<1$, with $m'=\alpha$, based on a recursive pole/zero placement in the frequency domain.

As mentioned in section 2, the Laplace definition for a derivative of order $\alpha \in C$ is a 'direct' generalization of the classical integer-order scheme with the multiplication of the signal transform by the s operator. Therefore, in what concerns automatic control theory this means that frequency-based analysis methods have a straightforward adaptation to their fractional-order counterparts. Nevertheless, the implementation based on the Laplace definition (adopting the frequency domain) requires an infinite number of poles and zeros obeying a recursive relationship [4]. In a real approximation the finite number of poles and zeros yields a ripple in the frequency response and a limited bandwidth.

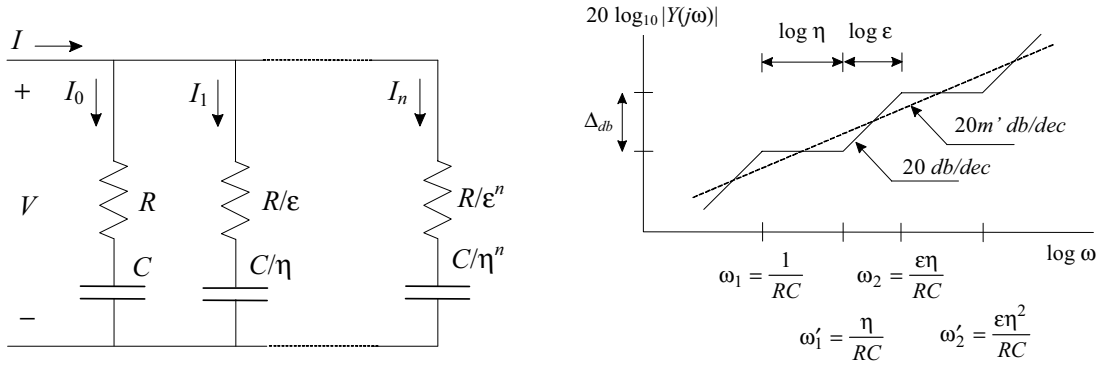

a) b)

Figure 1: a) Electrical circuit with a recursive association of resistances and capacitances; b) Bode diagram of amplitude of $Y(j\omega)$

Based on the Grünwald-Letnikov definition of a derivative of fractional order α of the signal $x(t)$, $D^{\alpha}x(t)$, leads to the expression:

$$D^{\alpha}x(t)=\lim_{h\to 0}\left[\frac{1}{h^{\alpha}}\sum_{k=0}^{\infty}(-1)^{k}\frac{\Gamma(\alpha+1)}{\Gamma(k+1)\Gamma(\alpha-k+1)}x(t-kh)\right] \tag{5}$$

where Γ is the gamma function and h is the time increment. This formulation [5] inspired a discrete-time calculation algorithm, based on the approximation of the time increment h through the sampling period T, yielding the equation in the z domain:

$$\frac{Z\left\{D^{\alpha}x(t)\right\}}{X(z)}\approx\frac{1}{T^{\alpha}}\sum_{k=0}^{\infty}\frac{(-1)^{k}\Gamma(\alpha+1)}{k!\,\Gamma(\alpha-k+1)}z^{-k}=\left(\frac{1-z^{-1}}{T}\right)^{\alpha} \tag{6}$$

An implementation of (6) corresponds to a r-term truncated series given by:

$$\frac{Z\left\{D^{\alpha}x(t)\right\}}{X(z)}\approx\frac{1}{T^{\alpha}}\sum_{k=0}^{r}\frac{(-1)^{k}\Gamma(\alpha+1)}{k!\,\Gamma(\alpha-k+1)}z^{-k} \tag{7}$$

Clearly, in order to have good approximations, we must have a large r and a small T.

An important aspect of fractional-order controllers can be illustrated through the elemental control system represented in Figure 2, with open-loop transfer function $G(s) = Ks^{-\alpha}$ ($1 < \alpha < 2$) in the forward path. The open-loop Bode diagrams (Figure 3) of amplitude and phase have a slope of -20α *dB*/*dec* and a constant phase of $-\alpha\pi/2$ *rad*, respectively. Therefore, the closed-loop system has a constant phase margin of $\pi(1 - \alpha/2)$ *rad*, that is independent of the system gain K. Likewise, this important property is also revealed through the root-locus depicted in Figure 4.

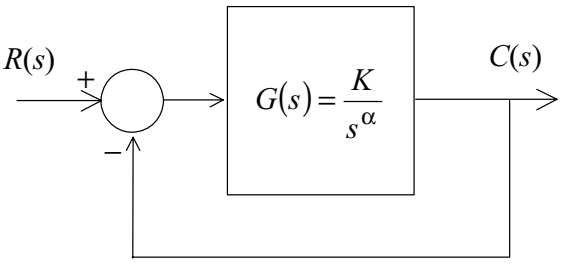

Figure 2: Block diagram for an elemental feedback control system of fractional order α

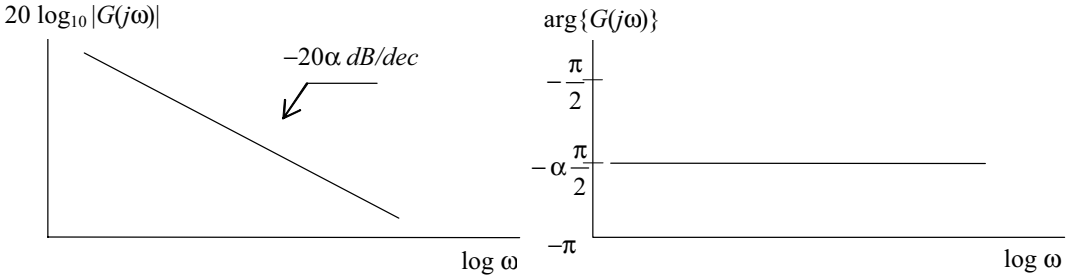

Figure 3: Open-loop Bode diagrams for a system of fractional order $1 < \alpha < 2$

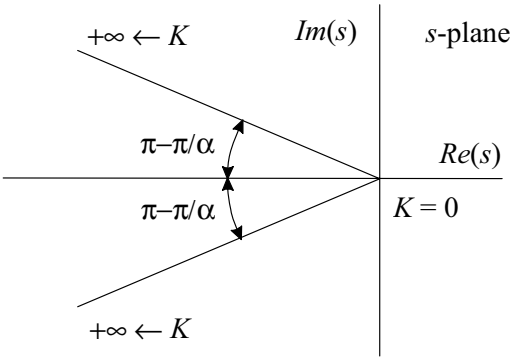

Figure 4: Root-locus for a feedback control system of fractional order $1 < \alpha < 2$

4 Control of Mechanical Systems

In this section we study the adoption of fractional-order algorithms in the dynamics and control of mechanical systems.

4.1 Describing Function of Systems with Backlash

The standard approach to the backlash study is based on the adoption of a geometric model that neglects the dynamic phenomena involved during the impact process. Due to this reason often real results differ significantly from those predicted by that model. In this section, we use the describing function (DF) method to analyse systems with backlash and impact phenomena [6], usually called *dynamic backlash*.

The proposed mechanical model consists on two masses (M_1 and M_2) with backlash and impacts as shown in Figure 5.

A collision between the masses M_1 and M_2 occurs when $x_1 = x_2$ or $x_2 = h + x_1$. In this case, we can compute the velocities of masses M_1 and M_2 after the impact ($\dot{x}_1'$ and $\dot{x}_2'$) by relating them to the previous values ($\dot{x}_1$ and $\dot{x}_2$) through Newton's rule:

$$\left(\dot{x}_1' - \dot{x}_2'\right) = -\varepsilon\left(\dot{x}_1 - \dot{x}_2\right), \quad 0 \le \varepsilon \le 1 \tag{8}$$

where ε is the coefficient of restitution. In the case of a fully plastic (*inelastic*) collision $\varepsilon = 0$, while in the *ideal elastic* case $\varepsilon = 1$.

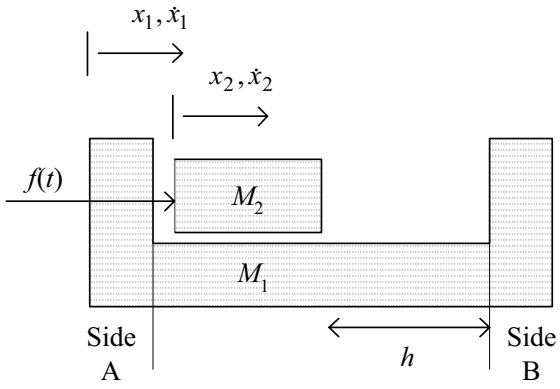

Figure 5: System with two masses subjected to dynamic backlash

By application of the principle of conservation of momentum $M_1\dot{x}_1' + M_2\dot{x}_2' = M_1\dot{x}_1 + M_2\dot{x}_2$ and of (8), we can find the sought velocities of both masses after an impact:

$$\dot{x}_1' = \frac{\dot{x}_1(M_1 - \varepsilon M_2) + \dot{x}_2(1+\varepsilon)M_2}{M_1 + M_2},\ \dot{x}_2' = \frac{\dot{x}_1(1+\varepsilon)M_1 + \dot{x}_2(M_2 - \varepsilon M_1)}{M_1 + M_2} \tag{9}$$

We can calculate numerically the Nyquist diagram of $-1/\mathrm{N}(F,\omega)$ for an input force $f(t) = F\cos(\omega t)$ applied to mass M_2 and an output position $x_1(t)$ of mass M_1.

Figure 6 shows the Nyquist plots for $F = 50$ N and $\varepsilon = \{0.1,\ldots,0.9\}$ and for $F = \{10, 20, 30, 40, 50\}$ N and $\varepsilon = 0.5$, respectively, considering $M_1 = M_2 = 1$ Kg and $h = 10^{-1}$ m. The charts reveal the occurrence of a jumping phenomenon, which is a characteristic of nonlinear systems. This phenomenon is more visible around $\varepsilon \approx 0.5$, while for the limiting cases ($\varepsilon \to 0$ and $\varepsilon \to 1$) the singularity disappears. Moreover, Figure 6b shows also that for a fixed value of ε the charts are proportional to the input amplitude F.

The validity of the model is restricted to an input force $f(t)$ with frequency higher than a lower-limit $\omega_C \approx [(2F/M_2h)^2(1-\varepsilon)^5]^{1/4}$ and lower than an upper-limit $\omega_L = 2(F/M_2h)^{1/2}$, corresponding to an amplitude of $x_1(t)$ within the clearance $h/2$. In the middle-range occurs a jumping phenomena at frequency $\omega_J \sim (F/M_2h)^{1/2}$.

Figure 7 shows the log-log plots of $\mathrm{Re}\{-1/\mathrm{N}\}$ and $\mathrm{Im}\{-1/\mathrm{N}\}$ *versus* ω with $F = 50$ N and $\varepsilon = \{0.1, 0.3, 0.5, 0.7, 0.9\}$, for the cases of the static and dynamic backlash.

The classical static backlash model corresponds to the DF of a linear system of a single mass M_1+M_2 followed by the geometric backlash having as input and as output the position variables. Comparing the results for the static and the dynamic backlash models we conclude that:

- The charts of $\mathrm{Re}\{-1/\mathrm{N}\}$ are similar for low frequencies (where they reveal a slope of +40 dB/dec) but differ significantly for high frequencies.
- The charts of $\mathrm{Im}\{-1/\mathrm{N}\}$ are different in all range of frequencies. Moreover, for low frequencies, the dynamic backlash has a fractional slope inferior to +80 dB/dec of the static model.

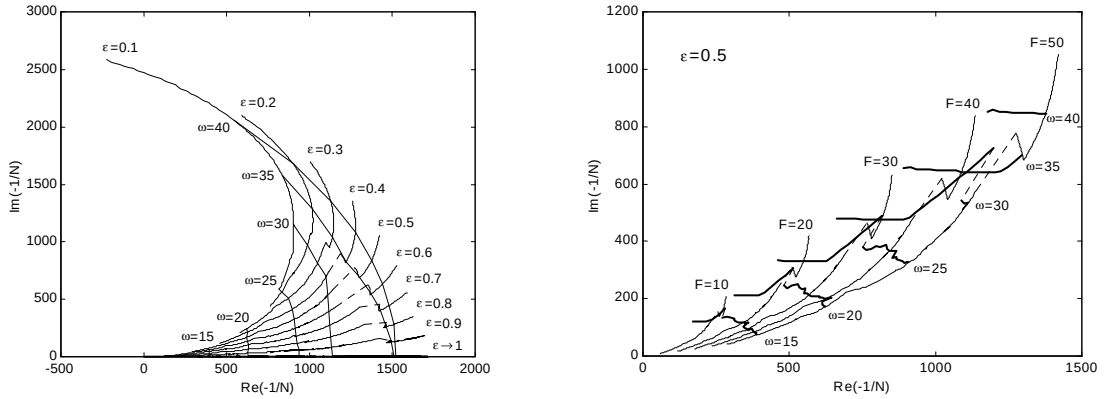

a) b)

Figure 6: Nyquist plot of $-1/\mathrm{N}(F,\omega)$ for a system with dynamic backlash, for: a) $F = 50$ N and $\varepsilon = \{0.1, \ldots, 0.9\}$; b) $F = \{10, 20, 30, 40, 50\}$ N and $\varepsilon = 0.5$

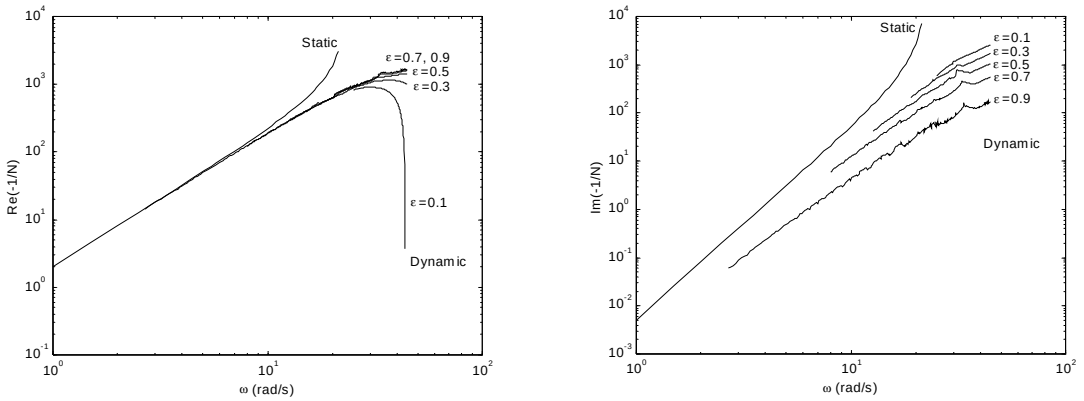

Figure 7: Plots of Re{−1/N(F,ω) } and Im{−1/N(F,ω) } for a system with dynamic backlash *versus* the exciting frequency ω, for F = 50 N and ε = {0.1, 0.3, 0.5, 0.7, 0.9}

A careful analysis must be taken because it was not demonstrated that a DF fractional slope would imply a fractional-order model. In fact, in this study we adopt integer-order models for the system description but the fractional-order slope is due to continuous/discrete dynamic variation that results due to the mass collisions [6].

4.2 Trajectory Control of Redundant Manipulators

A redundant manipulator possess more degrees-of-freedom (*dof*) than those required to establish an arbitrary position and orientation of the gripper. We consider a manipulator with n *dof* whose joint variables are denoted by $\mathbf{q} = [q_1,q_2,...,q_n]^{\mathrm{T}}$ and a class of operational tasks described by m variables $\mathbf{x} = [x_1,x_2,...,x_m]^{\mathrm{T}}$, $m < n$. The relation between the joint vector **q** and the manipulation vector **x** corresponds to the direct kinematics:

$$\mathbf{x} = f(\mathbf{q}) \tag{10}$$

Differentiating (10) with respect to time yields:

$$\dot{\mathbf{x}} = \mathbf{J}(\mathbf{q})\dot{\mathbf{q}} \tag{11}$$

Hence, from (11) it is possible to calculate a $\mathbf{q}(t)$ path in terms of a prescribed trajectory $\mathbf{x}(t)$. A solution is:

$$\dot{\mathbf{q}} = \mathbf{J}^{\#}(\mathbf{q})\dot{\mathbf{x}} \tag{12}$$

where $\mathbf{J}^{\#}$ is one of the generalized inverses of the **J**. The joint positions can be computed through the time integration of the velocities (12) according with the block diagram depicted in Figure 8.

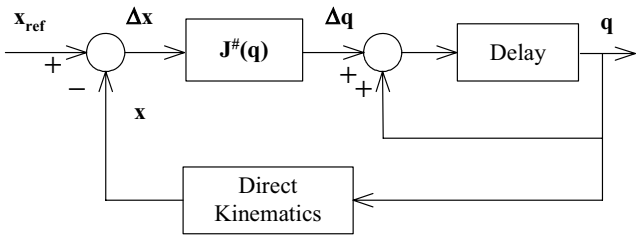

Figure 8: Diagram of the closed-loop inverse kinematics algorithm $\mathbf{J}^{\#}$

An important aspect is that repetitive trajectories in the operational space do not lead to periodic trajectories in the joint space. This is an obstacle for the solution of many tasks because the resultant robot configurations have similarities with those of a chaotic system.

We consider a 3*R* planar manipulator and during the experiments it is adopted $\Delta t = 10^{-3}$ s and $l_1 = l_2 = l_3 = 1$ m.

Figure 9 depicts the 3*R*-robot phase-plane joint trajectories, when repeating a circular motion with frequency $\omega_0 = 3$ rad/s, center at $r = [x^2+y^2]^{½} = 1$ m and radius $\rho = 0.1$ m. Besides the position and velocity drifts, leading to different trajectory loops, we have points that are 'avoided'. Such points correspond to arm configurations where several links are aligned.

In order to capture information about the system during all the dynamic evolution we devised an experiment that addresses the frequency response for two alternative exciting signals: a doublet-like and a white noise distributed throughout the 500-cycle trajectories. Figure 10 depicts the resulting amplitude Bode diagrams of the type:

$$\frac{Q_1(s)}{X_{ref}(s)} = K\frac{(s^{\alpha}+z)}{(s^{\alpha}+p)} \tag{13}$$

where K is the gain, z and p are the zero and pole, respectively, and α is the zero/pole fractional-order.

For the doublet excitation it results $\alpha \approx 1.0$ in contrast with the case of white noise excitation where we get a fractional value $\alpha \approx 1.3$. This is due to the memory-time property of fractional-order dynamics because they capture the dynamic phenomena involved during all the time-history of the experiment, in contrast with integer-order derivative that just capture a "local" dynamics [7].

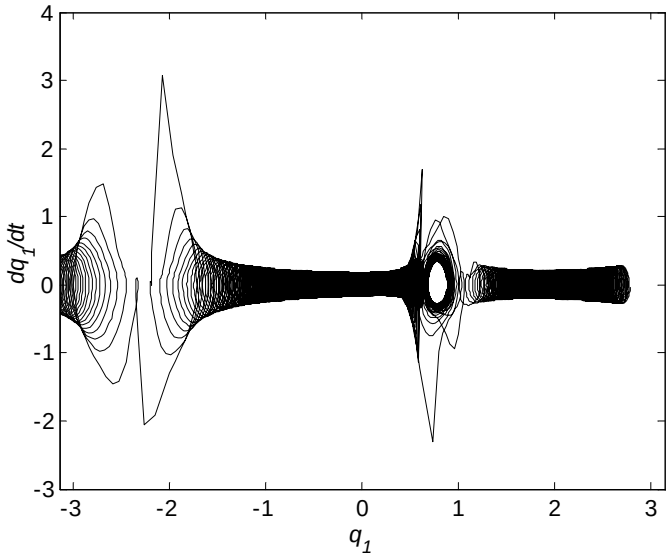

Figure 9: Phase plane trajectory for the 3*R*- robot joint 1 at $r = 1$ m, $\rho = 0.1$ m, $\omega_0 = 3$ rad/s

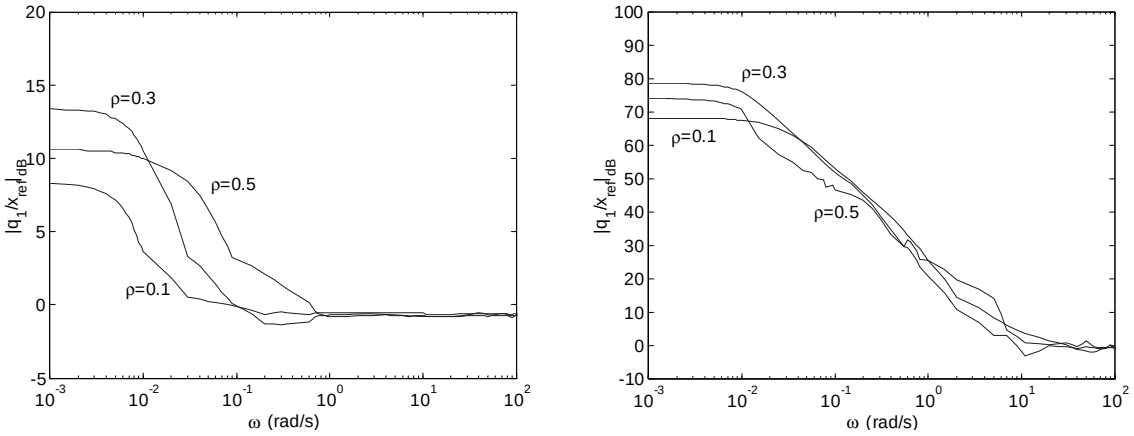

a) b)

Figure 10: Frequency response of the 3*R* robot $\omega_0 = 3$ rad/s, $r = 2$ m, $\rho \in \{0.10, 0.30, 0.50\}$ m for: a) A doublet-like; b) A white noise perturbation during 500-cycle trajectories

4.3 Position/Force Control of Manipulators

This section studies the position/force robot control, involving contact between the gripper and the environment, using fractional-order controllers in the hybrid algorithm proposed by Raibert and Craig [8].

The dynamical equation of an *n* dof robot interacting with the environment is given by:

$$\boldsymbol{\tau} = \mathbf{H}(\mathbf{q})\ddot{\mathbf{q}} + \mathbf{C}(\mathbf{q},\dot{\mathbf{q}}) + \mathbf{G}(\mathbf{q}) - \mathbf{J}^{\mathbf{T}}(\mathbf{q})\mathbf{F} \tag{14}$$

where $\boldsymbol{\tau}$ and $\mathbf{q}$ are the $n \times 1$ vectors of joint torques and positions, $\mathbf{H(q)}$ is the $n \times n$ inertia matrix, $\mathbf{C(q,\dot{q})}$ and $\mathbf{G(q)}$ are the $n \times 1$ vectors of centrifugal/Coriolis and gravitational terms and $\mathbf{F}$ is the $m \times 1$ vector of the force that the environment exerts in the gripper.

In this study we adopt the 2*R* robot (Fig. 11a) and we consider the schematic structure of the position/force hybrid control algorithm depicted in Fig. 11b.

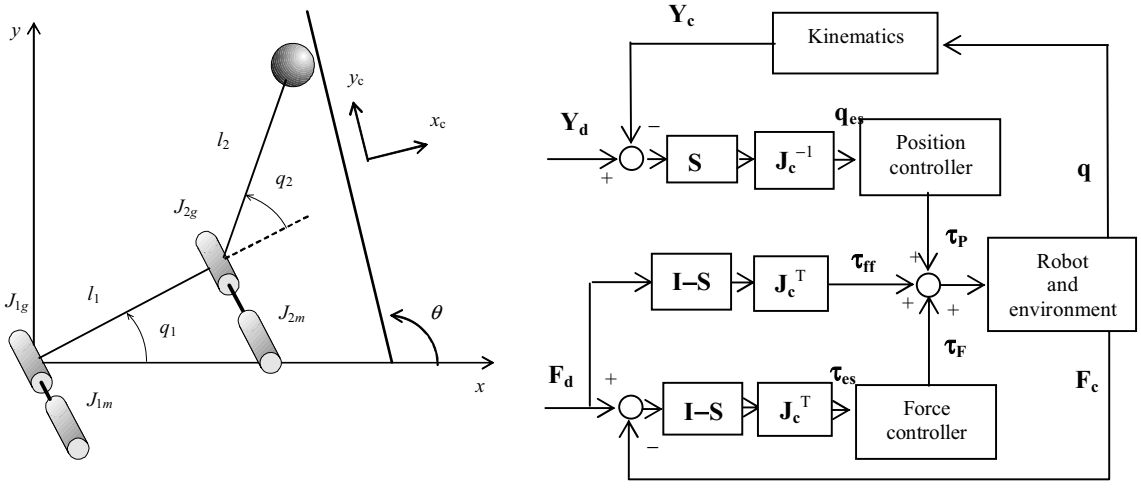

a) b)

Figure 11: a) 2*R* robot and constraint surface; b) Position/force hybrid controller

The numerical values adopted for the 2*R* robot are $m_1 = 0.5$ kg, $m_2 = 6.25$ kg, $r_1 = 1.0$ m, $r_2 = 0.8$ m, $J_{1m} = J_{2m} = 1.0$ kgm^2 and $J_{1g} = J_{2g} = 4.0$ kgm^2. In this paper we consider the y_C (x_C) Cartesian coordinates to be position (force) controlled.

The constraint plane is determined by the angle θ (Figure 11a) and the contact displacement x_c of the robot gripper with the constraint surface is modelled through a linear system with a mass *M*, a damping *B* and a stiffness *K* with dynamics:

$$F_c = M\ddot{x}_c + B\dot{x}_c + Kx_c \tag{15}$$

For comparison purposes we adopt fractional-order (*FO*) and *PID* algorithms for the position/force controllers. In our case, for implementing *FO* algorithms of the type $C(s) = K\,s^{\alpha}$, we adopt a 4$^{\text{th}}$-order discrete-time Padé approximation ($a_i, b_i, c_i, d_i \in R$, $n = 4$):

$$C_{\mathrm{P}}(z) \approx K_{\mathrm{P}}\,\frac{a_0 z^n + a_1 z^{n-1} + .. + a_n}{b_0 z^n + b_1 z^{n-1} + ... + b_n} \tag{16a}$$

$$C_{\mathrm{F}}(z) \approx K_{\mathrm{F}}\,\frac{c_0 z^n + c_1 z^{n-1} + .. + c_n}{d_0 z^n + d_1 z^{n-1} + ... + d_n} \tag{16b}$$

where $K_{\mathrm{P}}/K_{\mathrm{F}}$ are the position/force loop gains.

We analyze the system performance both for ideal transmissions and robots with backlash at the joints according with model (9). Moreover, we compare the response of *FO* and the *PD*: $C_{\mathrm{P}}(s) = K_p + K_d\,s$ and *PI*: $C_{\mathrm{F}}(s) = K_p + K_i\,s^{-1}$ controllers, in the position and force loops [9].

Both algorithms were tuned by trial and error having in mind getting a similar performance in the two cases. The resulting parameters were *FO*: $\{K_{\mathrm{P}},\alpha_{\mathrm{P}}\} \equiv \{10^5, 1/2\}$, $\{K_{\mathrm{F}},\alpha_{\mathrm{F}}\} \equiv \{10^3, -1/5\}$ and *PD*/*PI*: $\{K_p,K_d\} \equiv \{10^4,10^3\}$, $\{K_p,K_i\} \equiv \{10^3,10^2\}$ for the position and force loops, respectively. Moreover, it is adopted the operating point $\{x,y\} \equiv \{1,1\}$, a constraint surface with parameters $\{\theta,M,B,K\} \equiv \{\pi/2,10^3,1.0,10^2\}$ and a controller sampling frequency $f_{\mathrm{c}} = 1$ kHz.

In order to study the system dynamics we apply, separately, rectangular pulses, at the position and force references, that is, we perturb the references with $\{\delta y_{\mathrm{cd}},\delta F_{\mathrm{cd}}\} = \{10^{-1},0\}$ and $\{\delta y_{\mathrm{cd}},\delta F_{\mathrm{cd}}\} = \{0,10^{-1}\}$.

The time responses (Figures 12 and 13) reveal that, although tuned for similar performances in the first case, the *FO* is superior to the *PD/PI* in the cases with dynamical phenomena at the robot joints [9].

5 Conclusions

This paper presented the fundamental aspects of the FC calculus, the main approximation methods for the fractional-order derivatives calculation and the implication of the FC concepts on the extension of the classical automatic control theory. Bearing these ideas in mind, several motion control systems were described and their dynamics was analyzed in the perspective of fractional calculus. It was shown that fractional-order models capture phenomena and properties that classical integer-order simply neglect. In this line of thought, this article is a step towards the development of motion control systems based on the theory of FC.

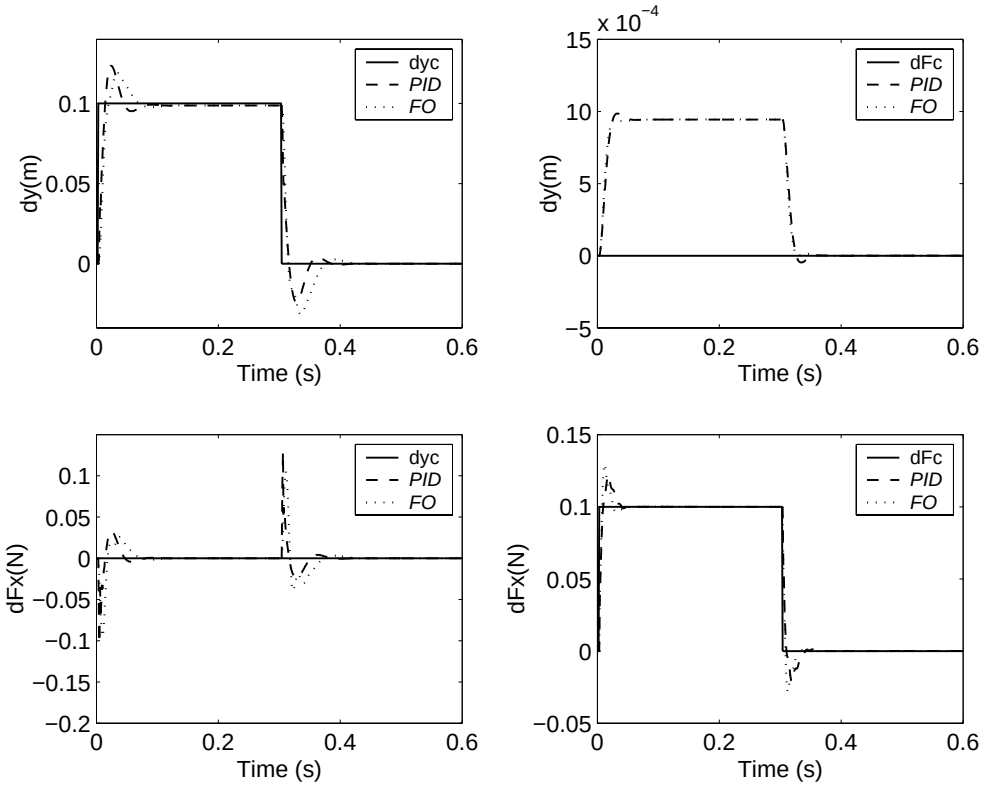

Figure 12: Time response for the 2*R* ideal robot with *FO* and *PD*/*PI* controllers

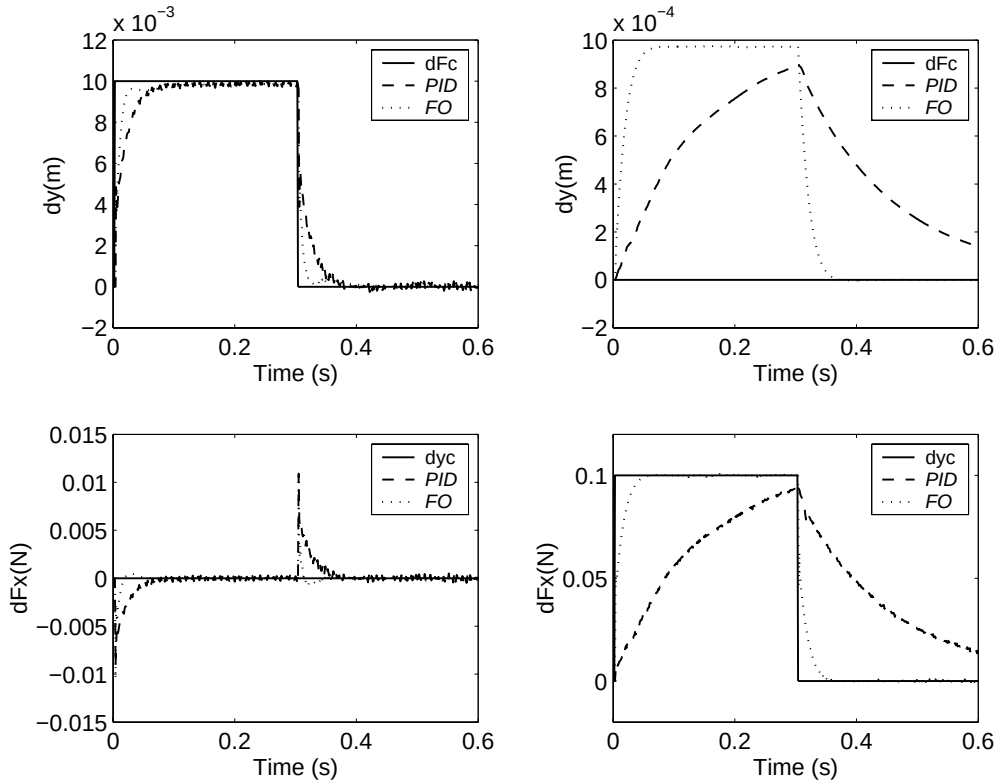

Figure 13: Time response for the 2*R* robot with backlash for *FO* and *PD*/*PI* controllers

References

[1] K. B. Oldham and J. Spanier. *The Fractional Calculus*. Academic Press, New York, 1974.

[2] K. S. Miller and B. Ross. *An Introduction to the Fractional Calculus and Fractional Differential Equations*. John Wiley and Sons, New York, 1993.

[3] S. G. Samko, A. A. Kilbas and O. I. Marichev. *Fractional Integrals and Derivatives*. Gordon and Breach Science Publishers, Amsterdam, 1993.

[4] A. Oustaloup. *La Dérivation Non Entière: Théorie, Synthèse et Applications*. Editions Hermes, Paris, 1995.

[5] J. A. Tenreiro Machado. Analysis and Design of Fractional-Order Digital Control Systems. *SAMS Journal Systems Analysis, Modelling, Simulation*, 27:107–122, 1997.

[6] Ramiro S. Barbosa and J. A. Tenreiro Machado. Describing Function Analysis of Systems with Impacts and Backlash. *Nonlinear Dynamics,* 29(1–4): 235–250, July 2002.

[7] Fernando B. Duarte and J. A. Tenreiro Machado. Chaotic Phenomena and Fractional-Order Dynamics in the Trajectory Control of Redundant Manipulators. *Nonlinear Dynamics,* 29(1–4): 315–342, July 2002.

[8] M. Raibert and J. Craig. Hybrid Position/Force Control of Manipulators. *ASME Journal of Dynamic Systems, Measurement, and Control*, 102(2): 126–133, 1981.

[9] J. A. Tenreiro Machado, Ramiro S. Barbosa, and N. M. Fonseca Ferreira. Fractional-Order Position/Force Control of Mechanical Manipulators. In *Proceedings of the CIFA'2002 - Conférence Int. Francophone d'Automatique*, pages 641–646, Nantes, France, July 2002.

About the Authors

J. A. T. Machado was born in 1957. He graduated and received the Ph.D. degree in electrical and computer engineering from the Faculty of Engineering of the University of Porto, Portugal, in 1980 and 1989, respectively. Presently he is Coordinator Professor at the Institute of Engineering of the Polytechnic Institute of Porto, Dept. of Electrical Engineering. His main research interests are robotics, modeling, control, genetic algorithms, fractional-order systems and intelligent transportation systems.

Ramiro Barbosa was born in 1971. He graduated in Electrical Engineering - Industrial Control from Institute of Engineering of Polytechnic Institute of Porto, Portugal, in 1994 and received the Master's degree in Electrical and Computer Engineering from the Faculty of Engineering of the University of Porto, Portugal, in 2000. Presently he teaches at the Institute of Engineering of the Polytechnic Institute of Porto, Dept. of Electrical Engineering. His research interests include modelling, control, fractional-order systems, and nonlinear systems.

Fernando Duarte was born in 1950. He graduated in Mathematics from University of Aveiro, Portugal, in 1982 and received the Ph.D. degree in Electrical and Computer Engineering from the Faculty of Engineering of the University of Porto, Portugal, in 2003. Presently he is Professor at the School of Technology, Polytechnic Institute of Viseu, Dept. of Mathematics. His main research interests are robotics, modeling, control, fractional-order systems.

Nuno Ferreira graduated with the B.A. degree in the Institute of Engineering of the Polytechnic Institute of Coimbra, in 1994, the degree in Electrotechnical Engineering at the University of Porto, in 1996 and the Master's degree in Electrotechnical and Computer Engineering in 1999. Presently he is Professor at the Institute of Engineering, Polytechnic Institute of Coimbra, Dept. of Electrotechnical Engineering. His main research interests are robotics and nonlinear systems.